Spin-liquid ground state in the frustrated J_1-J_2 zigzag chain system BaTb$_2$O$_4$

A. A. Aczel,[1,*] L. Li,[2] V. O. Garlea,[1] J.-Q. Yan,[2,3] F. Weickert,[4] V. S. Zapf,[4] R. Movshovich,[4] M. Jaime,[4] P. J. Baker,[5]
V. Keppens,[2] and D. Mandrus[2,3]

[1]*Quantum Condensed Matter Division, Oak Ridge National Laboratory, Oak Ridge, Tennessee 37831, USA*
[2]*Department of Materials Science and Engineering, University of Tennessee, Knoxville, Tennessee 37996, USA*
[3]*Materials Science and Technology Division, Oak Ridge National Laboratory, Oak Ridge, Tennessee 37831, USA*
[4]*MPA-CMMS, Los Alamos National Laboratory, Los Alamos, New Mexico 87545, USA*
[5]*ISIS Facility, STFC Rutherford Appleton Laboratory, Harwell Oxford, Oxfordshire OX11 0QX, United Kingdom*

We have investigated polycrystalline samples of the zigzag chain system BaTb$_2$O$_4$ with magnetic susceptibility, heat capacity, neutron powder diffraction, and muon spin relaxation (μSR). No magnetic transitions are observed in the bulk measurements, while neutron diffraction reveals the presence of low-temperature, short-range, intrachain magnetic correlations between Tb^{3+} ions. μSR indicates that these correlations are dynamic, as no signatures of static magnetism are detected by the technique down to 0.095 K. These combined findings provide strong evidence for a spin-liquid ground state in BaTb$_2$O$_4$.

Spin liquids are exotic ground states of frustrated magnets in which local moments are highly correlated but still fluctuate strongly down to zero temperature [1]. In principle, the fluctuations of a spin liquid can be quantum or classical in nature. Several types of spin liquids have been proposed theoretically, including Anderson's resonating valence bond state [2], spin ice [3,4], and others characterized by either gapped or gapless low-energy excitations [5]. The experimental search for new spin-liquid candidates is an ongoing area of interest since this state of matter remains largely unexplored in the laboratory. Some well-known examples of quantum spin-liquid candidates include ZnCu$_3$(OH)$_6$Cl$_2$ (herbertsmithite) [6,7], BaCu$_3$V$_2$O$_8$(OH)$_2$ (vesignieite) [8], and Ba$_3$NiSb$_2$O$_9$ [9], while their classical counterparts are the pyrochlore magnets Ho$_2$Ti$_2$O$_7$ and Dy$_2$Ti$_2$O$_7$ [1,10,11].

Magnetic systems characterized by frustration and low dimensionality have proven to be useful starting points in the quest for uncovering additional spin liquids, but particular complications have severely limited the number of viable candidates. For example, although one-dimensional (1D) magnets and two-dimensional Heisenberg systems are not expected to order due to the Mermin-Wagner theorem [12], most real low-dimensional materials are governed by weak exchange interactions in the other spatial dimensions and therefore exhibit magnetic order at low temperatures. Furthermore, although magnetic frustration can prevent leading terms in the Hamiltonian from selecting a conventional ordered ground state, there are instances in which the subleading terms can still drive the system to an ordered spin configuration [13]. To overcome these obstacles and find new spin-liquid candidates, it is important to perform detailed studies on a wide variety of frustrated, low-dimensional magnets.

The family of materials AR_2O_4 (A = Ba, Sr; R = rare earth) [14–16] satisfy the two criteria described above. Two crystallographically inequivalent R sites independently form two different types of zigzag chains [17–19] running along

---
*Author to whom correspondence should be addressed: aczelaa@ornl.gov

the c axis, as shown by the schematics in Fig. 1(a), and therefore quasi-1D magnetic behavior may be expected. Bulk characterization studies have also shown that most members of the family have dominant antiferromagnetic (AFM) exchange interactions and relatively large frustration indices. Geometric frustration can arise in this structure type if the J_2 exchange interactions are AFM and the J_1 couplings are of comparable strength. Note that the two chain types may have inequivalent J_1 and J_2 interactions.

The general expectation for the AR_2O_4 family, according to theoretical predictions of the classical zigzag chain [20,21] with AFM J_1 and J_2 couplings, is that a small (large) ionic radius [22] r for the R atom will decrease (increase) the J_1 distance and induce Néel (double Néel or helimagnetic) order on the chains. Schematics of the Néel and double Néel magnetic order, with the latter state expected in the large AFM J_2 limit of the Ising zigzag chain, are shown in Fig. 1(a). The zigzag chain framework has served as a good starting point for understanding the AR_2O_4 ground states, as Néel and double Néel long-range order have been observed in the systems with the smallest and largest R ionic radii studied with neutron scattering (SrYb$_2$O$_4$, $r = 0.87$ Å [23] and BaNd$_2$O$_4$, $r = 0.98$ Å [24]). However, a variety of magnetic phases have been discovered in the intermediate regime for the R ionic radii that are not easily explained by previous theoretical work. These phases include coexisting long-range Néel and short-range double Néel order in SrEr$_2$O$_4$ ($r = 0.94$ Å) [17,25], coexisting short-range Néel and short-range double Néel order in SrHo$_2$O$_4$ ($r = 0.90$ Å) [19,26,27], incommensurate magnetic order in SrTb$_2$O$_4$ ($r = 0.92$ Å) [28], short-range magnetic order in SrDy$_2$O$_4$ ($r = 0.91$ Å) [18,29], and no magnetic ordering of any kind in SrTm$_2$O$_4$ ($r = 0.88$ Å) [30]. It is also interesting to note that long-range order observed in this family has often been found to arise from only one rare earth site. Since the J_1 and J_2 exchange path distances are essentially equal for the two chain types, this behavior may be a consequence of the inequivalent, distorted oxygen octahedral local environments of the rare earths comprising each chain.

In this Rapid Communication, we extend previous investigations of the AR_2O_4 family with intermediate R ionic radii
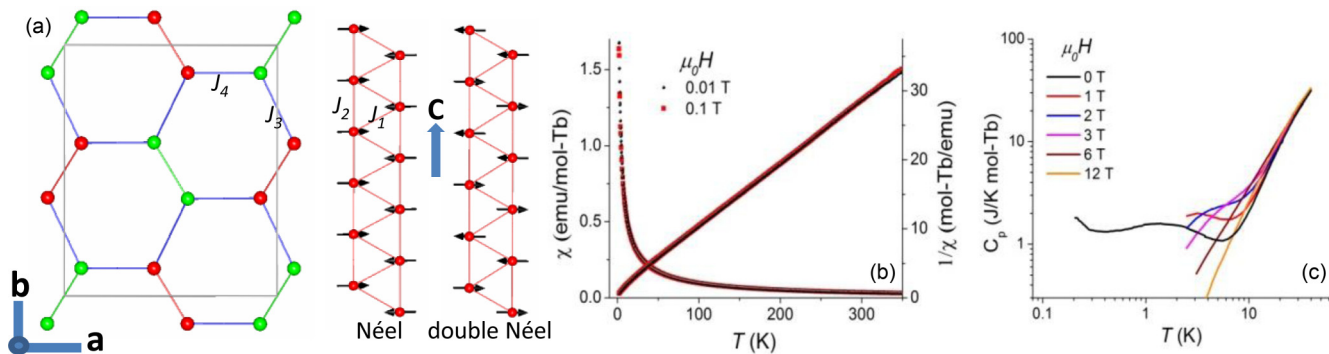
FIG. 1. (Color online) (a) Schematic of the *ab* plane for the AR_2O_4 structure, showing the R atoms only. The two inequivalent sites are illustrated in different colors. Schematics of the zigzag chain are also presented, showing both the Néel and double Néel ground states that arise from the classical J_1-J_2 Ising model in the strong AFM J_1 and J_2 limits, respectively. (b) Magnetic susceptibility of $BaTb_2O_4$, showing no evidence for long-range order down to 2 K. (c) C_p data measured between 0 and 12 T are shown on a double logarithmic scale with no indication of magnetic order. The low-temperature peak centered at $T^* = 1.5$ K in zero field is likely due to a low-lying crystal field level.

to polycrystalline $BaTb_2O_4$ ($r = 0.92$ Å) by performing a combination of magnetic susceptibility, heat capacity, neutron diffraction, and muon spin relaxation measurements on this system. The magnetic species is Tb^{3+}, which is a non-Kramers ion with a large angular momentum $J = 6$. We find no evidence for long-range magnetic ordering or spin freezing in any of our measurements down to 0.095 K. However, neutron diffraction reveals the presence of extremely short-range, intrachain magnetic correlations at temperatures below the modulus of the Curie-Weiss temperature $|\theta_{CW}| = 18$ K, extending up to next nearest neighbor Tb^{3+} ions at most. These findings provide compelling evidence that $BaTb_2O_4$ is a spin-liquid candidate.

Polycrystalline $BaTb_2O_4$ was synthesized by using the procedure presented in the Supplemental Material [31]. The magnetic susceptibility χ of polycrystalline $BaTb_2O_4$ was measured in applied fields $\mu_0 H = 0.01$ and 0.1 T using a Quantum Design magnetic properties measurement system. The data are presented in Fig. 1(b), with $\chi = M/\mu_0 H$ (magnetization/applied field), and the results are in reasonable agreement with previous work [15]. The high-temperature data is well described by a Curie-Weiss law, with a fit between 150 and 350 K yielding $\theta_{CW} = -18$ K and an effective moment $\mu_{eff} = 9.55 \mu_B$. The effective moment is close to the expected value of $9.72 \mu_B$ for Tb^{3+}. There is no evidence for long-range magnetic order from the χ measurements down to 2 K. Zero-field-cooled and field-cooled data were collected from 2 to 50 K, and no signatures of spin freezing are found either.

The specific heat (C_p) below 2 K was measured with a home-built probe based on the adiabatic heat-pulse technique in a ^{3}He/^{4}He dilution refrigerator from Oxford Instruments. Data at higher temperatures were taken in a Quantum Design physical properties measurement system equipped with a 12 T superconducting magnet. Figure 1(c) shows C_p data in selected applied fields. No evidence for magnetic order is found, while the observed field dependence is likely indicative of crystal field splitting that changes with $\mu_0 H$.

The zero-field C_p data show a sharp upturn for $T < 0.3$ K that can be attributed to nuclear Schottky contributions of Tb [32,33] or Ba nuclei. A broad maximum is also observed at $T^* = 1.5$ K, which likely corresponds to a low-lying

crystal field level. To estimate the entropy recovered on warming through this peak, the lattice contribution C_{lat} was first determined by fitting the C_p data from 20 to 40 K (where the field dependence is minimal) to the function $C_{lat} = AT^3 + BT^5 + DT^7$ and then subtracted off. Integrating the remaining contribution C_{mag}/T for $T > 0.3$ K yields an entropy of 4.9(1) J/K mol Tb. The recovered entropy is between the values of $R \ln(3)$ and $R \ln(4)$ assuming it corresponds to one Tb site only, or close to $R \ln(2)$ if both Tb sites are considered. It is difficult to make specific conclusions from the entropy analysis, due to the monoclinic site symmetries and the inequivalence of the local environments for the two different Tb sites. The buildup of magnetic correlations with decreasing T can also complicate this analysis [34].

Neutron powder diffraction was performed with 5 g of polycrystalline $BaTb_2O_4$ between 0.3 and 300 K at Oak Ridge National Laboratory using the HB-2A powder diffractometer of the High Flux Isotope Reactor with a collimation of 12′-open-6′. Data with a neutron wavelength of 2.41 Å are depicted in Figs. 2(a) and 2(d) with $T = 0.3$ and 10 K, respectively. Successful Rietveld refinements were performed using FULLPROF [35] with the known room-temperature space group *Pnam* [15], indicating that there are no structural phase transitions down to 0.3 K. The lattice constants at 0.3 K are refined as $a = 10.4226(2)$ Å, $b = 12.1784(2)$ Å, and $c = 3.4965(1)$ Å. Detailed structure information obtained from refinements of the $T = 300$ and 0.3 K data can be found in the Supplemental Material [31].

No evidence was found for long-range order in the diffraction data of $BaTb_2O_4$. However, magnetic diffuse scattering was observed instead in both the 0.3 and 10 K data sets. The diffuse scattering is modeled as background in Figs. 2(a) and 2(d), and most clearly seen in Figs. 2(b) and 2(e). The Q dependence of this scattering remains almost unchanged up to 10 K. These findings indicate that there are significant magnetic correlations that persist well above the onset of any possible long-range order. We note that the combined diffraction and susceptibility data rule out a well-isolated crystal field singlet ground state as found for $Tm_2Ti_2O_7$ [36] and possibly applicable to $SrTm_2O_4$ [30], since the signatures for such a scenario are a constant low-T
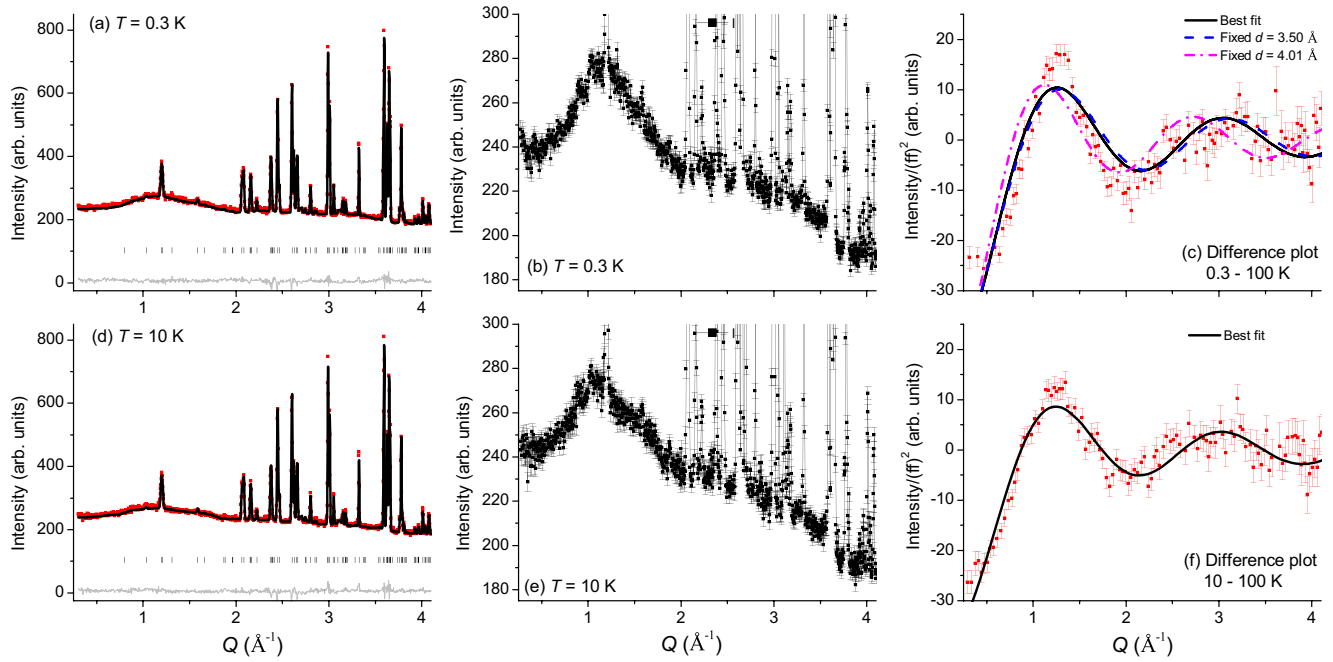
FIG. 2. (Color online) (a) HB-2A neutron diffraction data with $\lambda = 2.41$ Å at 0.3 K for polycrystalline $BaTb_2O_4$. The solid curve is a fit generated from a structural Rietveld refinement using the space group *Pnam*. (b) An enlarged version of the data shown in (a), emphasizing the magnetic diffuse scattering. (c) A 0.3–100 K difference plot, with the intensity normalized by the Tb^{3+} magnetic form factor squared. The curves are fits to various models that include magnetic correlations between Tb^{3+} ions separated by one particular distance only. (d)–(f) Similar plots to those shown in (a)–(c), but with $T = 10$ K.

magnetic susceptibility and the absence of any elastic magnetic scattering, in contrast to observations.

The 0.3–100 and 10–100 K difference plots are shown in Figs. 2(c) and 2(f), with the data normalized by the Tb^{3+} form factor squared. We verified that 100 K was a suitable background temperature by finding no evidence for magnetic correlations in the raw data (not shown). Similar oscillatory scattering patterns are clearly evident in both difference plots, therefore no drastic change is found in the correlation length through T^*. The intensity of the difference plots was fit to the function

$$I(Q) = \sum_{ij} A_{ij} \frac{\sin(Qd_{ij})}{Qd_{ij}}, \tag{1}$$

which has proven to be a useful starting point for describing short-range magnetic correlations in several different systems [37–42]. This equation represents the expected polycrystalline response for a local magnetic structure with isotropic interactions; the spins at sites i and j are correlated over a distance of d_{ij}. Antiferromagnetic (ferromagnetic) correlations are inferred from $A_{ij} < 0$ ($A_{ij} > 0$). In $BaTb_2O_4$, the 0.3 K refinement discussed above yields a J_2 distance of 3.50 Å, while the two types of zigzag chains are found to have inequivalent J_1 distances of 3.59 and 3.62 Å. The shortest interchain distance in the system corresponds to the J_4 exchange path, which has a length of 4.01 Å.

The best fits of the $BaTb_2O_4$ data, shown by the solid curves in Figs. 2(c) and 2(f), require only one term with $A < 0$ and $d = 3.58(4)$ Å at 0.3 K [3.61(3) Å at 10 K]. These fits correctly account for the positions of the peaks and valleys in the diffuse scattering. The inclusion of additional terms incorporating

larger Tb-Tb distances does not improve the quality of the fitting. We note that the lack of perfect agreement between the best fits and our data may be due to the role that magnetic anisotropy plays in $BaTb_2O_4$—a similar conclusion was made for $Tb_2Ti_2O_7$ [38,43]. Single component fits for $BaTb_2O_4$ are also shown in Fig. 2(c) with d fixed to 3.50 and 4.01 Å, and they show that the overall agreement with the data is very similar in the former case and significantly worse for the latter. Based on these combined findings, the strongest conclusion we can make from this data is that short-range, intrachain AFM correlations are present in $BaTb_2O_4$, extending up to next nearest neighbors at most. Furthermore, since the magnetic diffraction pattern for $BaTb_2O_4$ can be modeled with only one local magnetic structure, this implies that the two Tb^{3+} sites host very similar magnetic ground states or one of them has a nonmagnetic singlet ground state.

The observation of magnetic diffuse scattering in neutron diffraction studies alone does not allow one to determine whether the moments are truly static or dynamic in the magnetic ground state. For example, diffuse scattering was observed in diffraction measurements of the pyrochlore systems $Tb_2Mo_2O_7$ [37] and $Tb_2Ti_2O_7$ [38], but the molybdate has been characterized as a spin glass [44] while the titanate is a quantum spin ice candidate [45]. Muon spin relaxation (μSR) measurements [46] proved to be instrumental in searching for the evidence of spin freezing needed to differentiate between spin glass and more exotic dynamic ground states in these pyrochlore systems [38,47].

Therefore, to better understand the magnetic ground state of $BaTb_2O_4$, μSR was performed at the EMU (10–300 K) and MuSR (0.095–4 K) spectrometers in longitudinal field
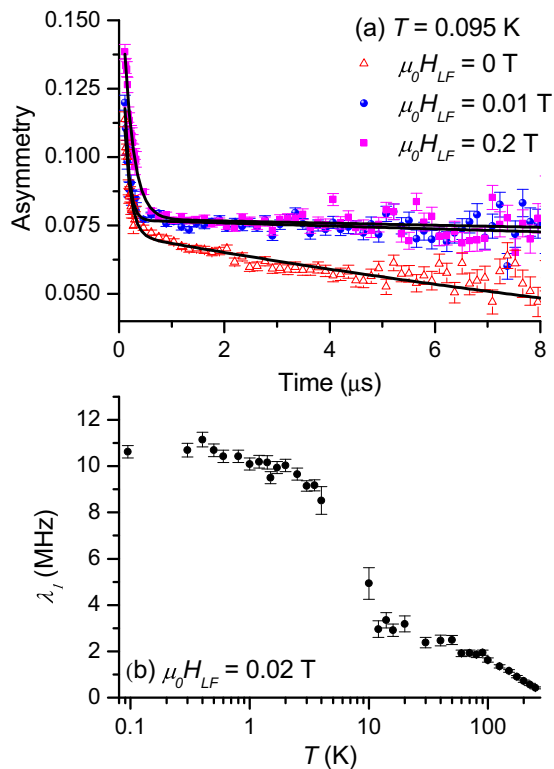
FIG. 3. (Color online) (a) μSR spectra collected in selected LFs at 0.095 K, with fits indicated by the solid lines, as described in the text. Very little decoupling of the zero-field relaxation is observed up to 0.2 T, which suggests that its origin is a dynamic mechanism. (b) T dependence of the relaxation rate λ_1, which saturates below 1 K. This T dependence is consistent with dynamic behavior of the moments down to the lowest temperatures investigated.

(LF) geometry at the ISIS Pulsed Neutron and Muon Source. Zero-field data were collected at 0.095, 0.5, 2, and 4 K, and no features characteristic of long-range order or spin freezing were observed. Data were also collected in several different LFs at 0.095 K. Some selected spectra are shown in Fig. 3(a), and they fit well to the expression

$$A(t) = A_1 e^{-\lambda_1 t} + A_B e^{-\lambda_B t}, \qquad (2)$$

where the two terms represent muons that stop in the sample and the sample holder, respectively.

Assuming the magnetic fields experienced by muons in $BaTb_2O_4$ are static, then their magnitude can be estimated from the zero-field μSR data by using the approximation $B_{loc} = \lambda_1/\gamma_\mu$, where $\gamma_\mu = 135.5 \times 2\pi$ MHz/T is the muon gyromagnetic ratio. In the present case, this analysis yields $B_{loc} = 0.0125$ T for the lowest temperatures studied. However, this description is incompatible with the form of the data arising from LF measurements at low temperature. If the muon

spin relaxation in zero field was caused by a static mechanism, then a LF around one order of magnitude larger than the local field should be sufficient to completely decouple the relaxing signal. Figure 3(a) shows that this is the case for the relaxation from the sample holder, but quite the opposite is true for the relaxation from the sample contribution. In fact, the sample component of the $\mu_0 H_{LF} = 0.2$ T spectrum shows only modest changes from the zero-field case. This implies that the muon spin relaxation arising from the sample has a dynamic origin and rules out a static spin-glass-like ground state for $BaTb_2O_4$.

μSR spectra were also collected with $\mu_0 H_{LF} = 0.02$ T at a variety of different temperatures to allow for an accurate measurement of $\lambda_1 = 1/T_1$. Figure 3(b) depicts the T dependence of $1/T_1$. No sharp peak is observed as would be expected in the case of spin freezing [47]; $1/T_1$ saturates below $\sim$1 K instead. A single exponential muon spin relaxation rate from the sample is also observed at all temperatures. These findings are indicative of large, rapidly fluctuating internal magnetic fields, as expected for a paramagnet [38,46], and they are in good agreement with the decoupling scheme observed in the LF scan at 0.095 K.

Our combined data are consistent with a cooperative paramagnetic or spin-liquid ground state for $BaTb_2O_4$, as we have found evidence for extremely short-range, dynamic, intrachain magnetic correlations between Tb^{3+} ions that persist down to 0.095 K. Theoretical models based on the classical zigzag chain with J_1 and J_2 intrachain exchange alone cannot explain the origin of this exotic state. Additional measurements and theoretical work are needed to understand the role that interchain interactions, single ion anisotropy, dipolar interactions, and the crystal field level schemes for the two Tb^{3+} sites play in the ground state selection for this material.

[1] L. Balents, Nature (London) **464**, 199 (2010).

[2] P. W. Anderson, Science **235**, 1196 (1987).

[3] S. T. Bramwell and M. J. P. Gingras, Science **294**, 1495 (2001).

[4] M. J. P. Gingras, in *Highly Frustrated Magnetism*, edited by C. Lacroix, P. Mendels, and F. Mila (Springer, Berlin, 2009).

[5] X.-G. Wen, Phys. Rev. B **65**, 165113 (2002).

[6] J. S. Helton, K. Matan, M. P. Shores, E. A. Nytko, B. M. Bartlett, Y. Yoshida, Y. Takano, A. Suslov, Y. Qiu, J. H. Chung, D. G. Nocera, and Y. S. Lee, Phys. Rev. Lett. **98**, 107204 (2007).

[7] T.-H. Han, J. S. Helton, S. Chu, D. G. Nocera, J. A. Rodriguez-Rivera, C. Broholm, and Y. S. Lee, Nature (London) **492**, 406 (2012).

[8] Y. Okamoto, H. Yoshida, and Z. Hiroi, J. Phys. Soc. Jpn. **78**, 033701 (2009).

[9] J. G. Cheng, G. Li, L. Balicas, J. S. Zhou, J. B. Goodenough, C. Xu, and H. D. Zhou, Phys. Rev. Lett. **107**, 197204 (2011).

[10] M. J. Harris, S. T. Bramwell, D. F. McMorrow, T. Zeiske, and K. W. Godfrey, Phys. Rev. Lett. **79**, 2554 (1997).

[11] A. P. Ramirez, A. Hayashi, R. J. Cava, R. Siddharthan, and B. S. Shastry, Nature (London) **399**, 333 (1999).

[12] N. D. Mermin and H. Wagner, Phys. Rev. Lett. **17**, 1133 (1966).

[13] N. P. Raju, M. Dion, M. J. P. Gingras, T. E. Mason, and J. E. Greedan, Phys. Rev. B **59**, 14489 (1999).

[14] H. Karunadasa, Q. Huang, B. G. Ueland, J. W. Lynn, P. Schiffer, K. A. Regan, and R. J. Cava, Phys. Rev. B **71**, 144414 (2005).

[15] Y. Doi, W. Nakamori, and Y. Hinatsu, J. Phys.: Condens. Matter **18**, 333 (2006).

[16] T. Besara, M. S. Lundberg, J. Sun, D. Ramirez, L. Dong, J. B. Whalen, R. Vasquez, F. Herrera, J. R. Allen, M. W. Davidson, and T. Siegrist, Prog. Solid State Chem. **42**, 23 (2014).

[17] T. J. Hayes, G. Balakrishnan, P. P. Deen, P. Manuel, L. C. Chapon, and O. A. Petrenko, Phys. Rev. B **84**, 174435 (2011).

[18] A. Fennell, V. Y. Pomjakushin, A. Uldry, B. Delley, B. Prevost, A. Desilets-Benoit, A. D. Bianchi, R. I. Bewley, B. R. Hansen, T. Klimczuk, R. J. Cava, and M. Kenzelmann, Phys. Rev. B **89**, 224511 (2014).

[19] J.-J. Wen, W. Tian, V. O. Garlea, S. M. Koohpayeh, T. M. McQueen, H.-F. Li, J.-Q. Yan, J. A. Rodriguez-Rivera, D. Vaknin, and C. L. Broholm, Phys. Rev. B **91**, 054424 (2015).

[20] F. Heidrich-Meisner, I. A. Sergienko, A. E. Feiguin, and E. R. Dagotto, Phys. Rev. B **75**, 064413 (2007).

[21] T. Hikihara, M. Kaburagi, H. Kawamura, and T. Tonegawa, J. Phys. Soc. Jpn. **69**, 259 (2000).

[22] R. D. Shannon, Acta Crystallogr., Sect. A **32**, 751 (1976).

[23] D. L. Quintero-Castro, B. Lake, M. Reehuis, A. Niazi, H. Ryll, A. T. M. N. Islam, T. Fennell, S. A. J. Kimber, B. Klemke, J. Ollivier, V. G. Sakai, P. P. Deen, and H. Mutka, Phys. Rev. B **86**, 064203 (2012).

[24] A. A. Aczel, L. Li, V. O. Garlea, J.-Q. Yan, F. Weickert, M. Jaime, B. Maiorov, R. Movshovich, L. Civale, V. Keppens, and D. Mandrus, Phys. Rev. B **90**, 134403 (2014).

[25] O. A. Petrenko, G. Balakrishnan, N. R. Wilson, S. de Brion, E. Suard, and L. C. Chapon, Phys. Rev. B **78**, 184410 (2008).

[26] O. Young, L. C. Chapon, and O. A. Petrenko, J. Phys.: Conf. Ser. **391**, 012081 (2012).

[27] O. Young, A. R. Wildes, P. Manuel, B. Ouladdiaf, D. D. Khalyavin, G. Balakrishnan, and O. A. Petrenko, Phys. Rev. B **88**, 024411 (2013).

[28] H.-F. Li, C. Zhang, A. Senyshyn, A. Wildes, K. Schmalzl, W. Schmidt, M. Boehm, E. Ressouche, B. Hou, P. Meuffels, G. Roth, and T. Brückel, Front. Phys. **2**, 42 (2014).

[29] T. H. Cheffings, M. R. Lees, G. Balakrishnan, and O. A. Petrenko, J. Phys.: Condens. Matter **25**, 256001 (2013).

[30] H.-F. Li, B. Hou, A. Wildes, A. Senyshyn, K. Schmalzl, W. Schmidt, C. Zhang, T. Brückel, and G. Roth, arXiv:1404.0044.

[31] See Supplemental Material at http://link.aps.org/supplemental/10.1103/PhysRevB.92.041110 for brief description of $BaTb_2O_4$ polycrystalline synthesis and detailed structure parameters determined from neutron diffraction.

[32] C. A. Catanese, A. T. Skjeltorp, H. E. Meissner, and W. P. Wolf, Phys. Rev. B **8**, 4223 (1973).

[33] H. W. J. Blote, R. F. Wielinga, and W. J. Huiskamp, Physica (Amsterdam) **43**, 549 (1969).

[34] B. D. Gaulin, J. S. Gardner, P. A. McClarty, and M. J. P. Gingras, Phys. Rev. B **84**, 140402(R) (2011).

[35] J. Rodriguez-Carvajal, Physica B **192**, 55 (1993).

[36] M. P. Zinkin, M. J. Harris, Z. Tun, R. A. Cowley, and B. M. Wanklyn, J. Phys.: Condens. Matter **8**, 193 (1996).

[37] J. E. Greedan, J. N. Reimers, C. V. Stager, and S. L. Penny, Phys. Rev. B **43**, 5682 (1991).

[38] J. S. Gardner, S. R. Dunsiger, B. D. Gaulin, M. J. P. Gingras, J. E. Greedan, R. F. Kiefl, M. D. Lumsden, W. A. MacFarlane, N. P. Raju, J. E. Sonier, I. Swainson, and Z. Tun, Phys. Rev. Lett. **82**, 1012 (1999).

[39] B. Fak, F. C. Coomer, A. Harrison, D. Visser, and M. E. Zhitomirsky, Eur. Phys. Lett. **81**, 17006 (2008).

[40] P. M. Sarte, H. J. Silverstein, B. T. K. Van Wyk, J. S. Gardner, Y. Qiu, H. D. Zhou, and C. R. Wiebe, J. Phys.: Condens. Matter **23**, 382201 (2011).

[41] B. G. Ueland, C. F. Miclea, K. Gofryk, Y. Qiu, F. Ronning, R. Movshovich, E. D. Bauer, J. S. Gardner, and J. D. Thompson, Phys. Rev. B **90**, 121109(R) (2014).

[42] B. G. Ueland, J. S. Gardner, A. J. Williams, M. L. Dahlberg, J. G. Kim, Y. Qiu, J. R. D. Copley, P. Schiffer, and R. J. Cava, Phys. Rev. B **81**, 060408(R) (2010).

[43] J. S. Gardner, B. D. Gaulin, A. J. Berlinsky, P. Waldron, S. R. Dunsiger, N. P. Raju, and J. E. Greedan, Phys. Rev. B **64**, 224416 (2001).

[44] B. D. Gaulin, J. N. Reimers, T. E. Mason, J. E. Greedan, and Z. Tun, Phys. Rev. Lett. **69**, 3244 (1992).

[45] M. J. P. Gingras and P. A. McClarty, Rep. Prog. Phys. **77**, 056501 (2014), and references therein.

[46] P. D. de Reotier and A. Yaouanc, J. Phys.: Condens. Matter **9**, 9113 (1997).

[47] S. R. Dunsiger, R. F. Kiefl, K. H. Chow, B. D. Gaulin, M. J. P. Gingras, J. E. Greedan, A. Keren, K. Kojima, G. M. Luke, W. A. MacFarlane, N. P. Raju, J. E. Sonier, Y. J. Uemura, and W. D. Wu, Phys. Rev. B **54**, 9019 (1996).